ISOL-Method in Studies of Medium-Heavy $Z \sim N$ Nuclei

J. Huikari

Academic Dissertation
for a Degree of
Doctor of Philosophy

To be presented, by a permission of the
Faculty of Mathematics and Natural Sciences
of the University of Jyväskylä,
for a public examination in auditorium FYS-1
of the University of Jyväskylä on December 12, 2003
at 12 o'clock noon.

ISBN 978-951-39-3148-3
URN:ISBN:978-951-39-3148-3

Preface

The experimental work for this thesis has been carried out during the years 1998-2003 at the IGISOL facility in the Accelerator laboratory of Jyväskylä and at the ISOLDE facility in Cern, Geneva. I would like to thank the whole staff of the Department of Physics in Jyväskylä for creating an inspiring working atmosphere. Especially, I want to thank the workshop and cyclotron crew for their professional support which has made the experiments succesful and the secretaries for their readiness to help.

The IGISOL group has been an endless source of motivation for completing this work. I want to thank my supervisor, professor Juha Äystö, for confidence at the beginning and encouragement and guidance at the end of this project. The guidance and infinite patience of Dr. Peter Dendooven during my early years at IGISOL helped me to learn about the nature of the ion guides. Working with Dr. Arto Nieminen, Mr. Sami Rinta-Antila, Dr. Markku Oinonen, Dr. Andrey Popov, Dr. Kari Peräjärvi, Dr. Heikki Penttilä and Dr. Ari Jokinen has been both productive and lots of fun. Their calm style and sense of humour has created pleasent working conditions during these intensive years. In addition, there would not have been spectroscopic data available for analysis without Dr. Pete Jones whose contribution is gratefully acknowledged.

Finally, I want to thank my parents for their support and especially my wife Kristiina for her love and my daughter Aino for kindly reminding that there is a life outside the target hall.

Jyväskylä, December 2003
Jussi Huikari

Abstract

The β decay of ^{74}Rb, ^{75}Sr and ^{80m}Y was studied by means of β-delayed γ-ray and proton spectroscopy. The experiments were performed using the mass separator facilities at ISOLDE at CERN in Geneva and at IGISOL in Jyväskylä. Production rates of radioactive ions at IGISOL were studied extensively. A new interpretation of the ion guide efficiency dependence on the primary beam intensity is presented. The experimental results show that placing a ring electrode between the nozzle and the skimmer removes the earlier measured square root dependence. The first γ-γ coincidence measurement was carried out for ^{74}Rb where the 1198 keV transition was found to be in coincidence with the 456 keV ground state transition. The measurement of the branching ratios to excited states of ^{74}Kr allowed the improved determination of the intensity of the analog β decay. Therefore, the value for the total Coulomb correction $\delta_C = 2.4(3)$ % could be extracted. The study of ^{75}Sr resulted in an improved half-life 88(3) ms. Also, the first β-delayed γ transition was detected. The measurement of the β-delayed proton intensity allowed the determination of the Gamow-Teller strength distribution. The shape of the Gamow-Teller distribution suggests prolate deformation for the ^{75}Sr ground state. The accurate conversion coefficient measurement for ^{80m}Y confirmed the spin and parity of this isomer to be $I^\pi = 1^-$. As a consequence, during rp-process ^{80}Zr β decay populates the isomeric state. Thus, the proton capture takes place in the isomer, not in the ground state as previously assumed.

Contents

Enclosed articles:

Production rates of radioactive ions at IGISOL
J. Huikari, P. Dendooven, A. Jokinen, A. Nieminen, H. Penttilä, K. Peräjärvi, A. Popov, S. Rinta-Antila, J. Äystö, submitted to *Nucl. Instr. and Meth. Phys. Res. B*

Non-analog β decay of ^{74}Rb
M. Oinonen, J. Äystö, P. Baumann, J. Cederkäll, S. Courtin, P. Dessagne, S. Franchoo, H. Fynbo, M. Górska, J. Huikari, A. Jokinen, A. Knipper, U. Köster, G. Le Scornet, C. Miehé, A. Nieminen, T. Nilsson, Yu. Novikov, K. Peräjärvi, E. Poirier, A. Popov, D. M. Seliverstov, T. Siiskonen, H. Simon, O. Tengblad, P. Van Duppen, G. Walter, L. Weissman, K. Wilhelmsen-Rolander, *Phys. Lett. B 511 (2001) 145.*

Mirror decay of ^{75}Sr
J. Huikari, M. Oinonen, A. Algora, J. Cederkäll, S. Courtin, P. Dessagne, L. Fraile, S. Franchoo, H. Fynbo, W. X. Huang, A. Jokinen, A. Knipper, F. Marechal, C. Miehé, E. Nacher, K. Peräjärvi, E. Poirier, L. Weissman, J. Äystö and the ISOLDE Collaboration, *Eur. Phys. J. A 16 (2003) 359.*

Isomeric state of ^{80}Y and its role in the astrophysical rp-process
Yu. Novikov, H. Schatz, P. Dendooven, R. Béraud, C. Miehé, A. Popov, D. M. Seliverstov, G. K. Vorobjev, P. Baumann, M. J. G. Borge, G. Canchel, P. Dessagne, A. Emsallem, W. X. Huang, J. Huikari, A. Jokinen, A. Knipper, V. S. Kolhinen, A. Nieminen, M. Oinonen, H. Penttilä, K. Peräjärvi, I. Piqueras, S. Rinta-Antila, J. Szerypo, Y. Wang, and J. Äystö, *Eur. Phys. J. A 11 (2001) 257.*

1 Introduction

The nucleus can be characterised by several quantities. Some of these are the number of protons Z, the number of neutrons N, mass $A = N + Z$, isospin $T_z = (N\text{-}Z)/2$, the total angular momentum J, and the decay Q-value which is the mass difference of the parent and daughter nuclei. The study of these properties has advanced from the nuclei close to the valley of stability towards the so-called driplines, where the nuclei are no more stable against proton or neutron emissions. The exact location of the driplines is not certain as the predictions are based on the extrapolations from known nuclei. Various models have been developed for these predictions and these predictions differ considerably from each other. In addition, new phenomena are expected to occur in the nuclei far from stability. The changes in the shell structure have been predicted, and first hints of this have already been detected in the light nuclei for N = 20 and 28. Furthermore, a wide variety of different shapes of the nuclei has been discovered.

Fundamental interactions have presently been described by the Standard Model of electroweak interactions. Precise measurements of the nuclear β decay can be used for testing these interactions and symmetry laws. One of these tests is the unitarity of the Cabibbo-Kobayashi-Maskava quark-mixing matrix, which is one of the corner stones of the Standard Model. This test requires a very precise determination of half-lives, decay Q-values and branching ratios of superallowed β transitions. The required precision has been reached in a lower mass region up to ^{54}Co. Present efforts in this field are directed towards a deeper understanding of the quality of the isospin mixing corrections by extending the study to non-analogue transitions in higher-Z systems where the charge-dependent effects should be larger.

The nucleosynthesis in stars and during explosive stellar events like supernovae and X-ray bursts produces the elements which make up the universe. A complete description of the nucleosynthesis requires detailed knowledge of the nuclei and reactions in which they are involved. The astrophysical process which leads to the nucleosynthesis of proton-rich light and medium-mass nuclei is called the rapid proton capture (rp) process. The rp-process proceeds close to the proton dripline up to the tin region. The decay properties of the nuclei involved in the rp-process are reasonably well known below $Z = 35$. The nuclei with $Z > 35$ are known to be rich of isomers and deformations. As the isomers affect the effective half-lives and deformation affects the level structure, the theoretical predictions of the properties of these nuclei differ significantly.

The present work investigates nuclei near the $N = Z$ line in order to obtain information on the superallowed β decay of ^{74}Rb, mirror decay of ^{75}Sr as well as on the isomeric state of ^{80}Y, all located on the main rp-process path. In addition, as the β decay of ^{75}Sr has a sizeable Gamow-Teller part feeding the high lying states of ^{75}Rb it is a promising case for deformation studies.

As the nuclei studied in this thesis have short half-lives and they are located far from the valley of stability, advanced techniques are needed to produce them. For the

purposes of the present study, the Isotope Separator On-Line (ISOL) system originally developed in the 1960s for producing rare isotopes was used. In the ISOL system nuclei are produced, stopped, accelerated to an energy of a few tens of keV, and mass-separated in a continuous process.

As both the acceleration stage and mass-separation by a magnetic field require ions, the ion source is the most important device determining the ISOL performance. The ISOL concepts can be classified according to the way the reaction products are stopped. A schematic description of different ISOL concepts is presented in Fig. 1.

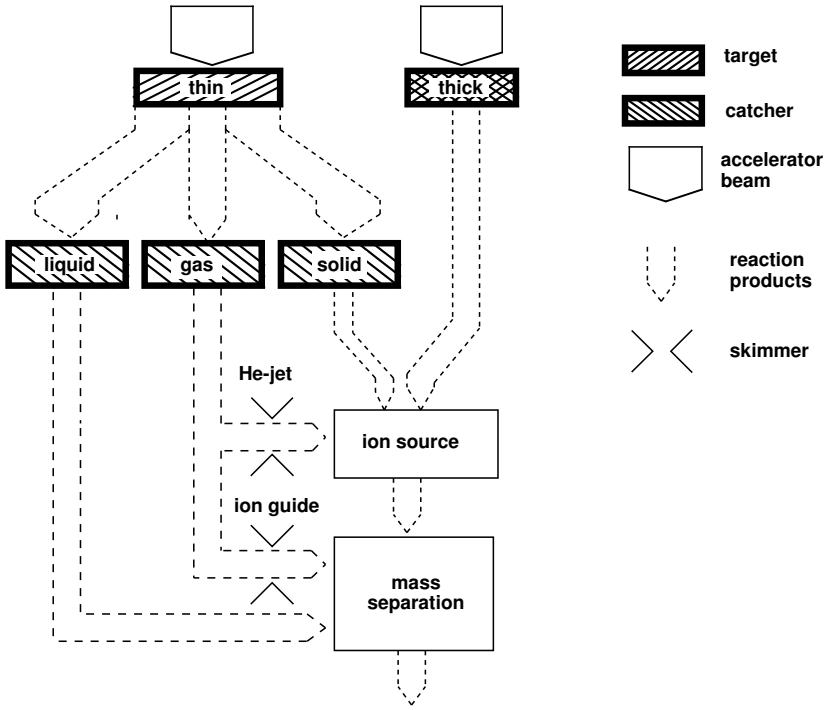

Figure 1: Different Isotope Separator On-Line (ISOL) concepts.

If the recoil range of the reaction products is small compared to the target thickness most of the reaction products are stopped in the target. When the targets used are thin most reaction products recoil out from the target. These recoils can be stopped in a solid catcher as in the GSI isotope separator [Roe03] or in a gaseous catcher as in IGISOL [A1]. If the target used is thick reaction products are stopped inside the target material. Two facilites using this technique are ISOLDE [ISO00] and TRIUMF-ISAC [Bri99]. Recently, the possibility to stop ions in liquid helium has been studied in the accelerator laboratory of Jyväskylä [Hua03]. Off-line experiments carried out show that ions can be extracted from liquid to vacuum as ions. This research is at its early stages and finding the means to transport ions to the accelerator stage is under investigation.

The reaction products stopped in solid material are released through diffusion and transported to an ion source. An efficient release of reaction products from solid material requires heating. Due to technical limits related to this method it is unsuitable for refractory elements. Furthermore, total separation times of less than one second are difficult to achieve, which has restricted the study of very short-living nuclei. Two different types of isotope separator were used to produce radioactive isotopes for the research discussed in the present thesis. These were IGISOL, where a gas catcher approach was used and ISOLDE, where a thick target approach was used. These isotope separators will be introduced in the following chapters.

The present work is based on the following enclosed publications:

A1. J. Huikari, P. Dendooven, A. Jokinen, A. Nieminen, H. Penttilä, K. Peräjärvi, A. Popov, S. Rinta-Antila, J. Äystö, Production rates of radioactive ions at IGISOL, submitted to Nucl. Instr. and Meth. Phys. Res. B.
The present author was actively involved in performing the experiments using a ^{223}Ra α-recoil source and participating in operating and developing the ion guide. He was the principal writer of the article.

A2. M. Oinonen, J. Äystö, P. Baumann, J. Cederkäll, S. Courtin, P. Dessagne, S. Franchoo, H. Fynbo, M. Górska, J. Huikari, A. Jokinen, A. Knipper, U. Köster, G. Le Scornet, C. Miehé, A. Nieminen, T. Nilsson, Yu. Novikov, K. Peräjärvi, E. Poirier, A. Popov, D. M. Seliverstov, T. Siiskonen, H. Simon, O. Tengblad, P. Van Duppen, G. Walter, L. Weissman, K. Wilhelmsen-Rolander, Non-analog β decay of ^{74}Rb, Phys. Lett. B 511 (2001) 145.
The present author performed a full data analysis on the conversion electron measurement for this article.

A3. J. Huikari, M. Oinonen, A. Algora, J. Cederkäll, S. Courtin, P. Dessagne, L. Fraile, S. Franchoo, H. Fynbo, W. X. Huang, A. Jokinen, A. Knipper, F. Marechal, C. Miehé, E. Nacher, K. Peräjärvi, E. Poirier, L. Weissman, J. Äystö and the ISOLDE Collaboration, Mirror decay of ^{75}Sr, Eur. Phys. J. A 16 (2003) 359.
The present author analysed the data, interpreted the results and wrote the article.

A4. Yu. Novikov, H. Schatz, P. Dendooven, R. Béraud, C. Miehé, A. Popov, D. M. Seliverstov, G. K. Vorobjev, P. Baumann, M. J. G. Borge, G. Canchel, P. Dessagne, A. Emsallem, W. X. Huang, J. Huikari, A. Jokinen, A. Knipper, V. S. Kolhinen, A. Nie- minen, M. Oinonen, H. Penttilä, K. Peräjärvi, I. Piqueras, S. Rinta-Antila, J. Szerypo, Y. Wang, and J. Äystö, Isomeric state of ^{80}Y and its role in the astrophysical rp-process, Eur. Phys. J. A 11 (2001) 257.
The present author's responsibility for this experiment was to prepare the IGISOL mass separator to provide a beam of ^{80}Y.

2 Experimental methods

2.1 IGISOL

The ion guide technique was developed in order to overcome the limitations related to the standard ISOL technique, namely the long delay time and a need for an ion source. The first system that can be called an ion guide isotope separator according to today's standards was developed at the Department of Physics in Jyväskylä. The first results were published in 1981 [Ärj81-1]. In this article, the term *ion guide* was introduced and the feasibility of the technique was shown off-line using a ^{227}Ac α-decay recoil source. The first on-line results, although without mass separation, were presented later in the same year at the EMIS-10 conference [Ärj81-2]. The first on-line mass separation was reported in 1983 [Ärj83-1] and was shortly followed by an application to nuclear structure physics [Äys84]. A general review of the ion guide technique in physics research is presented in [Äys01]. The development of the ion guide technique in Jyväskylä has led to three main types of ion guides: *light-ion ion guide*, *heavy-ion ion guide (HIGISOL)* and *fission ion guide*. The differences in their structure arise from the differences in reaction kinematics. The light-ion ion guide and HIGISOL are discussed in detail in the enclosed article A1. For a more detailed description of the fission ion guide, see Ref. [Tas89, Den00].

In the ion guide method, the projectile beam hits the thin target and product nuclei recoil out from the target as ions into a chamber filled with a stopping gas, which is usually helium. The charge state is proportional to the ion velocity. While the speed of the ions slows down their charge state changes continuously via charge exchange processes with the gas atoms. For most elements the second ionisation potential is lower than the first ionisation potential of helium. Therefore, in a pure atomic helium gas ions can only reach a 2^+ charge state in collisions with helium atoms. However, impurities such as O_2, N_2, Ne and H_2O often present in the system lead to charge transfer reactions with doubly charged ions. Thus, most of the ions end up in a 1^+ charge state. In addition, the ionisation of helium by the projectile beam increases the neutralisation rate due to a 3-body recombination between 1^+ ions, electrons, and helium atoms. Some ions are lost in the chamber due to diffusion to the chamber walls. The continuous helium flow carries thermalised reaction products out from the target chamber through the nozzle and the skimmer into the mass separator. The method is fast (sub ms) and chemically non-selective. Therefore, the refractory elements can also be mass separated. The present layout of the IGISOL facility is shown in Figure 2.

A typical feature with the ion guide has been a large energy spread, of the order of 100 eV, of the 40 keV mass separated beam. This has increased the background in the form of neighbouring masses as well as the reduction of the yield as the transmission efficiency through the separator decreases. In order to overcome this problem, the use

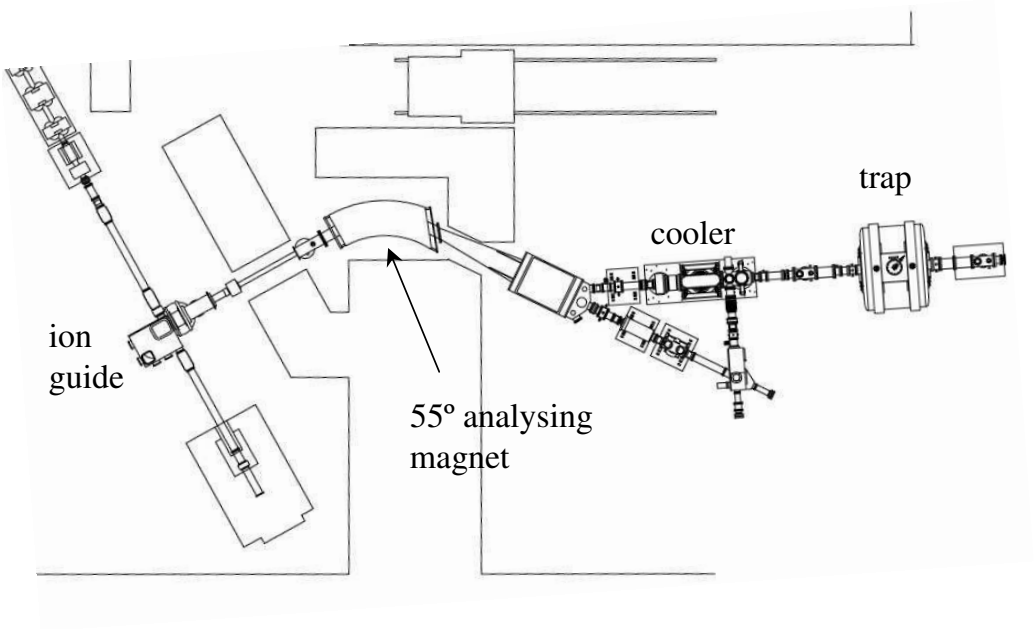

Figure 2: IGISOL facility.

of a sextupole ion guide, SPIG, has been studied with the fission and heavy-ion ion guides. The measured results show that the mass resolving power, M/ΔM, can be improved to 1100 when replacing the traditional skimmer with the SPIG. Moreover, there does not exist long tails in the mass peak. The production rates of the radioactive nuclei of the heavy-ion ion guide are slightly increased and the yields of the fission ion guide show significant improvement. The transportation capacity of the SPIG was measured to be of the order of 10^{12} ions/second.

When using the light-ion ion guide the efficiency has been dependent on the square root of the primary beam intensity. It was found out in this thesis that this square root dependence has been due to a decrease of the transportation efficiency between the exit hole and the skimmer. As a solution, the effect of a ring electrode between the skimmer and the ion guide exit hole was studied. The conclusion from these tests was that with the ring electrode the transmission efficiency between the skimmer and the exit hole can be maintained despite the large current flowing out from the ion guide. As a result, production rates improve as the efficiency does not drop when increasing the primary beam intensity.

In order to understand the processess inside the ion guide stopping volume, a ^{223}Ra α-recoil source was used to produce the ^{219}Rn beam. These studies consisted of delay time and efficiency mesurements as a function of ion guide pressure, source-to-exit-hole distance as well as buffer gas purity. The mass resolving power and absolute efficiency

of the ion-guide-SPIG system were also studied using the ^{219}Rn beam. The result was that the buffer gas composition should be matched to the chemical properties of the ion-of-interest. The proof of this is the measured charge state distribution of evacuated ions which can be influenced by the amount of impurities in the buffer gas.

The ^{223}Ra α-recoil source was used to test the idea of injecting electrons inside the stopping volume and, thus, improving the evacuation efficiency. An off-line test carried out showed that a factor of 10 increase of the efficiency can be achieved. However, on-line tests are required to measure whether this positive effect is present also with the presence of the plasma created by the ionising radiation.

2.2 ISOLDE

At the ISOLDE mass separator facility, radioactive nuclides are produced in a thick high-temperature target via spallation, fission or fragmentation reactions. The reaction products are released from the target via diffusion and effusion and guided through a tube to an ion source. This transfer tube can be cooled or heated depending on the properties of the element of interest. The target thickness is typically of the order of several g/cm^2. The target can be heated resistively up to 2400 C° depending on the materials used. The targets are placed in the external proton beam of the proton synchrotron booster, PSB, which has an energy of 1 or 1.4 GeV. PSB delivers a 2.4-μs-long proton pulse every 1.2 seconds. The intensity is $3.2{\cdot}10^{13}$ protons/pulse. Usually 6 pulses out from a 14.4 s supercycle are available for ISOLDE, which provides an average beam intensity of 2.1 μA. [ISO00] Figure 3 presents the layout of the ISOLDE facility.

The ISOLDE facility can presently offer three types of ion sources, namely laser ionising, surface ionising and plasma ion sources. A detailed description of the ISOLDE facility can be found from the ISOLDE laboratory portrait [ISO00].

The thickness of the Nb-foil target used in the present study to produce Sr and Rb was 50 g/cm^2. The ^{74}Rb and ^{75}Sr ions were ionised using a surface ionisation ion source. In the case of ^{75}Sr, CF_4 was added in order to suppress all the other elements except Sr from the mass separated beam. Thus, strontium was accelerated and mass separated as SrF^+ ions. Figure 4 presents Rb and Sr production rates at ISOLDE. The yields for ^{74}Rb and ^{75}Sr are from the present work and the rest are adopted from [ISOLDE]. The ^{74}Ga yield during the Rb experiment was 1 atom/μC. No isobaric background was detected during the Sr experiment.

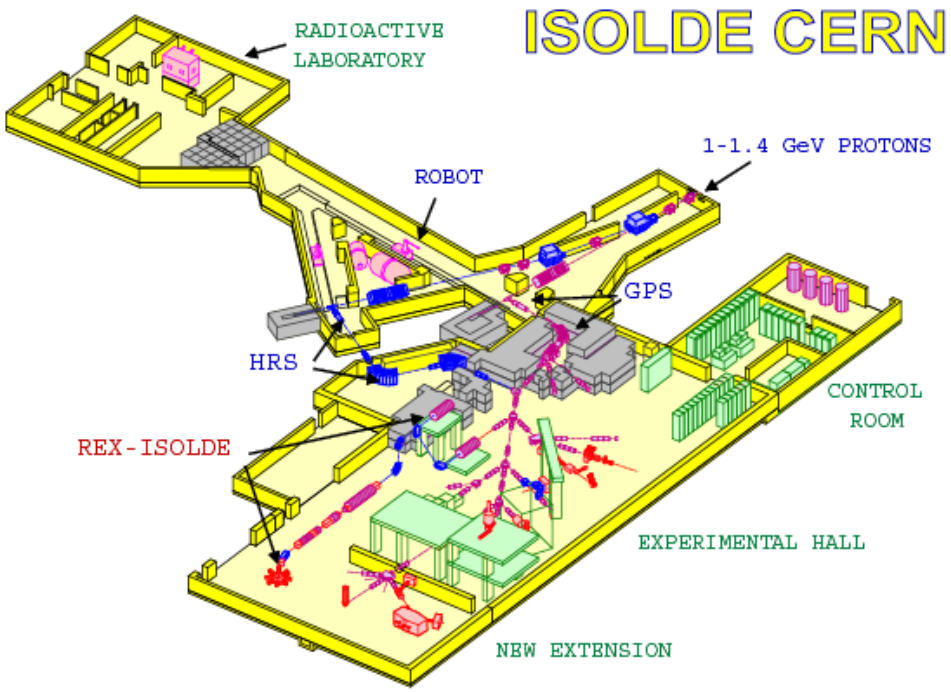

Figure 3: ISOLDE facility [ISOLDE].

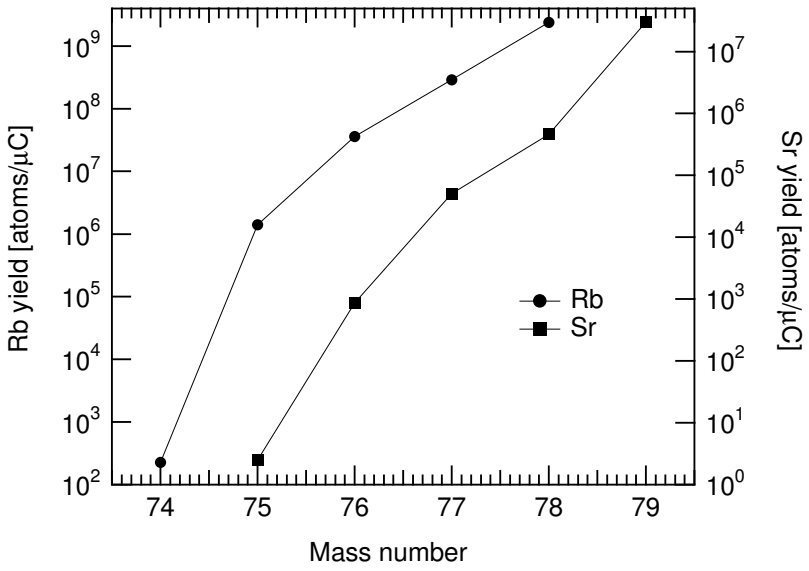

Figure 4: Rb and Sr production rates. Sr ions are all produced as SrF.

2.3 Detector set-ups

For the purposes of this thesis, the β decay of ^{74}Rb, ^{75}Sr and ^{80}Y was studied by means of β-delayed γ, conversion electron and proton spectroscopy. The topics of interest were β decay half-life, β decay energy and transition intensities to the excited states of daughter nuclei. The schematic drawings of the detector set-ups used in the experiments are presented in Figure 5.

For ^{74}Rb, three experiments were conducted. In the first one, the detector setup *a* was used. It consisted of a β telescope made of a 2-mm thick plastic scintillator and a planar Ge detector, a 70 % HPGe detector for γ-ray detection and a charged-particle detector telescope [Hon97]. This set-up was used to search for β-delayed protons. The set-up *b* was used in the second experiment for β-delayed γ-rays. In this experiment, a cylindrical scintillator with a 70 % efficiency was used as a trigger detector for β particles. The γ -rays were detected with three 70 % Ge detectors. Each Ge detector was equipped with a veto detector in front of the Ge crystal to reduce β-γ summing.

The set-up *c* used in the third experiment on ^{74}Rb β decay consisted of two 3-cluster MINIBALL [Ebe96] detectors and a 70 % efficiency cylindrical scintillator as a trigger detector for β particles. The purpose of this experiment was to measure β-delayed γ rays and look for γ-γ coincidences.

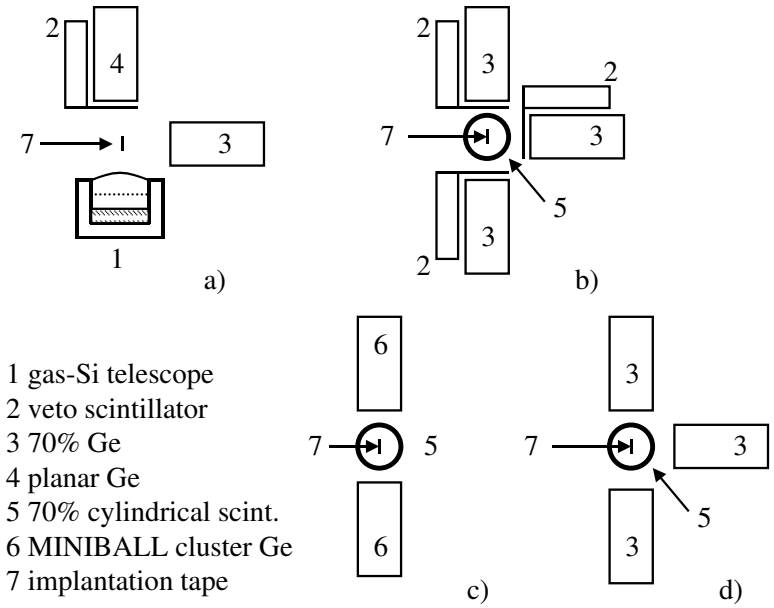

Figure 5: Detector set-ups used in different experiments of this thesis. a) ^{74}Rb β delayed protons, b) ^{74}Rb β decay half-life, c) ^{74}Rb β-delayed γ rays, d) ^{75}Sr β-delayed γ rays.

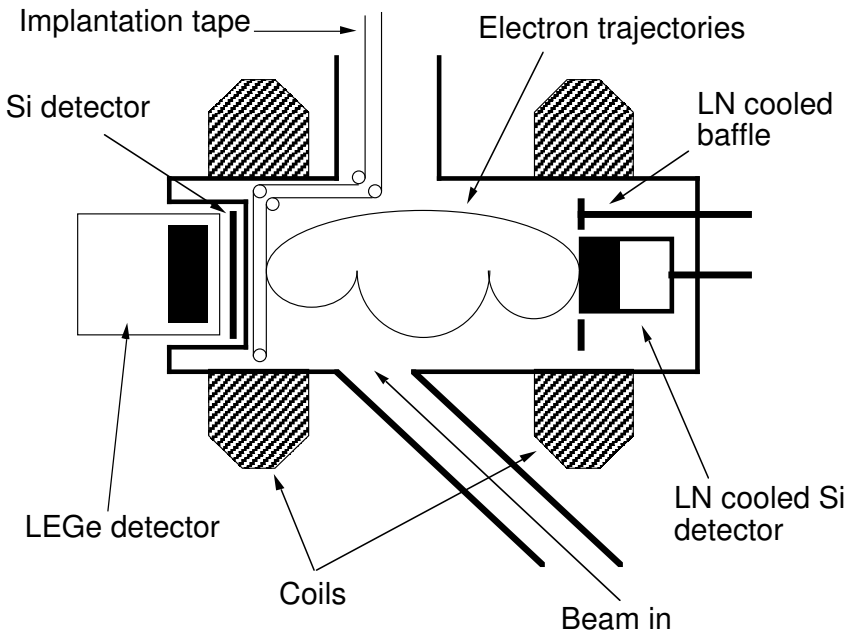

Figure 6: ELLI (ELectron Lens for IGISOL).

Conversion electrons were searched for using the magnetic conversion electron spectrometer ELLI (ELectron Lens for IGISOL) in coincidence with Si and Ge detectors. ELLI is a two-coil magnetic transporter which can provide extremely clean background conditions. The ions are implanted on the movable tape located on the first maximum of the magnetic field. The liquid nitrogen cooled SiLi detector is located on the second maximum of the magnetic field. A schematic drawing of this set-up is shown in Figure 6. For more details on ELLI, see [Par91].

In the ^{75}Sr experiment, the detection set-up used for the half-life and β-delayed γ rays consisted of the 70 % cylindrical plastic scintillator for β particles and three Ge detectors for γ rays (d in Figure 5). The set-up for β-delayed protons and γ rays consisted of the FUTIS array [Oin96] with 15 Si (300 μm) detectors, with a transmission type Si (500 μm) detector and a 20-mm-thick planar Ge detector behind the implantation position in close geometry. A drawing of the FUTIS array is shown in Figure 7. In all the experiments discussed in the present paper, ions were implanted on a aluminised mylar tape to be able to remove long living contaminants and daughter activities away from the counting position.

Efficiency calibrations for the detector set-ups used were carried out using the absolutely calibrated sources and on-line activities of known radioactive decays. The β-γ set-ups for ^{74}Rb and ^{75}Sr were calibrated using ^{152}Eu and ^{133}Ba sources. The absolute efficiency as well as the energy calibration for the ELLI set-up was obtained

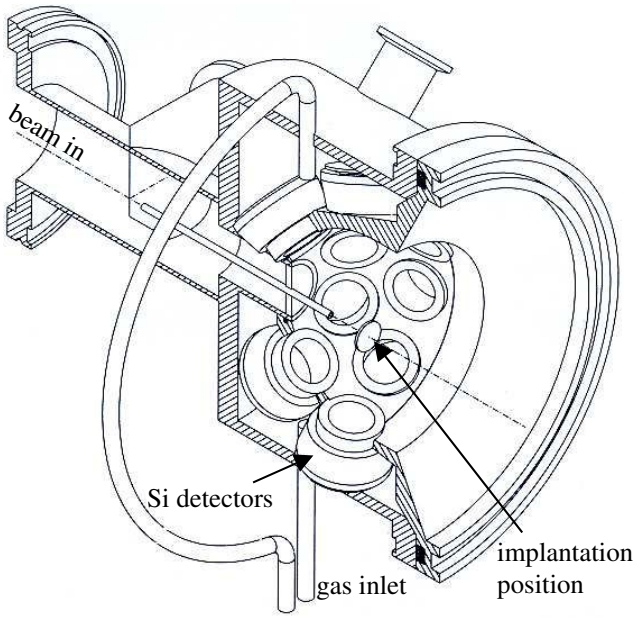

Figure 7: FUTIS.

using ^{133}Ba and ^{131}Ba calibration sources and ^{74}Kr, ^{77}Rb, ^{76}Rb and ^{77}Kr on-line sources produced at ISOLDE. The FUTIS array was calibrated using an on-line source of ^{20}Na. A ^{133}Ba source was used for the γ detector used in this measurement. The 1633 keV γ transition from ^{20}Na decay observed in the Ge detector was used to obtain the absolute efficiency of the FUTIS array. The Q_{EC} value for ^{75}Sr β decay was deduced from the β energy spectrum of the Ge detector. The energy calibration for this was determined using ^{62}Ga, ^{50}Mn and ^{20}Na on-line sources. The slope of the linear calibration curve was checked using neutron induced γ rays detected in the Ge detector.

In the ^{80}Y experiment, the detector set-up consisted of the ELLI spectrometer and the planar Ge detector in the same ways as in the ^{74}Rb experiment except that the Si detector in front of the Ge detector was not used. The on-line source ^{81}Y and ^{133}Ba calibration source were used determing the energy calibration and absolute efficiency and ^{241}Am was used to obtain the absolute efficiency for the Ge detector at low energies.

3 β decay and nuclear structure

3.1 General features of allowed β decay

β decay is a universal term for weak interaction transitions between two neighbouring nuclear isobars. It occurs in three forms, β^+, β^-, and electron capture (EC) decay. In each case, a nucleon inside the nucleus is transformed into another and a neutrino is

emitted. The maximum energy available for the β decay equals to the mass difference of the mother and daughter nuclei. The three-body characteristics of β decay which is caused by the presence of neutrino leads to a continuous energy spectrum for the emitted β particles.

The β-decay probability depends on the energy released in the decay, the angular momentum of the emitted particles, the nuclear charge and the nature of the initial and final nuclear states. Fermi's golden rule states that the transition rate between an initial and final state is given by

$$\lambda = \frac{2\pi}{\hbar}|M|^2\frac{dn}{dE}, \tag{1}$$

where E is the energy available for the final state products, dn/dE is the density of the final states and M is the matrix element. The term dn/dE is often referred to as the phase-space factor. [Lil01]

The Hamiltonian for the β decay consists of vector and axial-vector terms. In the approximation for allowed transitions the vector part of the interaction reduces to the unit operator *1* and the axial-vector term to the spin operator σ. In addition, the isospin raising/lowering operator $t_\pm$ has to be present as a proton is converted to a neutron in the β^+ decay. Both the vector and axial-vector interaction can contribute simultaneously. Hence, the β decay transition probability can be written as

$$\lambda \propto G_V^2\langle M_F\rangle^2 + G_A^2\langle M_{GT}\rangle^2, \tag{2}$$

where G_V and G_A are the vector and axial-vector coupling constants, respectively. [Bru77]

The squared matrix element M^2 for the Fermi β decay is

$$\langle M_F\rangle^2 = \langle 1\rangle^2 = \langle J_f M T_f M_{Tf}|1\sum_{k=1}^{A} t_\pm(k)|J_i M T_i M_{Ti}\rangle^2, \tag{3}$$

where J is the total spin, M is the magnetic quantum number, T is the isospin quantum number and M_T is the isospin projection. The subscripts i and f refer to initial and final states of the decay, respectively. The operator for the Fermi decay, $1\sum_{k=1}^{A} t_\pm(k) = 1T_\pm$, does not change the spin or parity. The Fermi transition affects only the isospin orientation. The model independent form of the Fermi matrix element can be obtained by normalisation of the wave functions and it can be written as

$$\langle 1\rangle^2 = T(T+1) - M_{Ti}M_{Tf}. \tag{4}$$

The squared matrix element for the Gamow-Teller β decay is

$$\langle M_{GT}\rangle^2 = \langle\sigma\tau\rangle^2 = \frac{1}{2J_i+1}\sum_{mM_iM_f}|\langle J_f M_f T_f M_{Tf}|\sum_{k=1}^{A}\sigma_m(k)t_\pm(k)|J_i M_i T_i M_{Ti}\rangle|^2. \tag{5}$$

The spin operator σ_m does not change the sign under parity operation. The Gamow-Teller matrix element cannot be expressed directly in terms of the total isospin as in the case of Fermi decay. However, the simplest form for the Gamow-Teller matrix element can be obtained by assuming an inert core with J=0, T=0 and a single active nucleon. As a result, an extreme single particle estimate (ESP) for the squared Gamow-Teller matrix element can be written as

$$\langle\sigma\tau\rangle^2 = 6(2j_f+1)\left\{ \begin{array}{ccc} \frac{1}{2} & \frac{1}{2} & 1 \\ j_i & j_f & l \end{array} \right\}^2, \tag{6}$$

where $\{\ldots\}$ is the 6j symbol, which is tabulated in [Bru77], for example.

Conservation of angular momentum and parity and the properties of the initial and final states determine the type of β decay that can occur. In Fermi decay the emitted positron and neutrino have antiparallel spins (S=0), and, therefore, no orbital angular momentum is carried away. In the Gamow-Teller decay, positron and neutrino spins are parallel (S=1), and one unit of angular momentum is carried away. Thus, the transitions must satisfy the following vector addition rules:

I_f	=	$I_i + L$	for Fermi transitions
I_f	=	$I_i + L + 1$	for Gamow-Teller transitions

The reduced β decay strength is often written as a comparable half-life, *ft*, where f is the statiscical rate function dependent on the daughter Z and the decay energy. In this equation, t is a partial half-life of a corresponding transition, t = λ/ln(2). The Fermi and Gamow-Teller matrix elements and the transition strengths in allowed decays are related as

$$(1+\delta_R)ft = \frac{C}{\langle 1\rangle^2(1-\delta_C) + (\frac{G_A}{G_V})^2\langle\sigma\tau\rangle^2}, \tag{7}$$

where δ_R is a radiative correction and δ_C a correction due to the isospin impurity. In the present work, the following values were used for these corrections:

(1+δ_R)	=	1.026	[Ewa81]
(1-δ_C)	=	0.997(3)	[Wil78]
C	=	6145(4)	[Tow95]
$\lvert G_A/G_V \rvert$	=	1.266(4)	[Sch95]

The log *ft* values can be used for classifying different types of β decay. Table 1 summarises the selection rules for spherical nuclei. The transition probability decreases with increasing L.

The allowed Fermi or mixed Fermi and Gamow-Teller transitions which have log *ft*-values between 2.9 and 3.7 are called superallowed transitions. Particularly, the log

Table 1: The β-decay selection rules for spherical nuclei [Kan95]. Transitions which are not possible if either I_i or I_f is zero are given in parenthesis. The limits for log *ft* values are from [Did94]

Transition type	log *ft*	L	Fermi		Gamow-Teller	
			ΔI	$\Delta\pi$	ΔI	$\Delta\pi$
Allowed	<5.9	0	0	No	(0),1	No
1st forbidden	>8.0	1	(0),1	Yes	0,1,2	Yes
2nd forbidden	>10.6	2	(1),2	No	2,3	No

ft value between the isobaric analog states for $0^+ \rightarrow 0^+$ (T = 1) transition is known as 3.49. The Fermi matrix element $\langle 1 \rangle^2$ vanishes unless $T_f = T_i$ and $M_{Tf} = M_{Ti} \pm 1$, where M is the isospin projection. Thus, the allowed Fermi decay occurs only between the isobaric analog states and it is the only possible decay mode for the $0^+ \rightarrow 0^+$ transitions between analog states.

3.2 Quasi-particle Random-Phase Approximation (QRPA)

The model based on single particle estimates has turned out to be too simple to describe nuclei between closed shells. Therefore, more sophisticated and elaborate methods are needed for theoretical predictions. Presently, the use of shell model calculations is limited by computing capacity to lower mass nuclei below the *fp* shell. The theoretical predictions used in the interpretation of the results from the ^{75}Sr β-decay work are based on pnQRPA calculations using a deformed selfconsistent HF+BCS basis with the Skyrme force SG2 and including consistent spin-isospin residual interactions [Sar01-1, Sar] and deformed HF-BCS with Skyrme interactions [Ham99].

QRPA has been succesful in the description of spherical and deformed nuclei within the valley of stability. In this method, the Skyrme interactions are determined by fits to global properties of spherical nuclei over the nuclear chart. Next, the gap parameters of the pairing force and the coupling strength of the residual neutron-proton pairing force are specified. Therefore, there are no free parameters left. Both the residual interaction and the mean field are obtained from the same two-body force. Therefore, this method can be considered suitable for extrapolations to the unstable nuclei approaching driplines.

The solution for the HF equations was based on the McMaster procedure, which assumes time reversal and axial symmetry. The single particle wave functions were expanded in terms of the eigenstates of an axially symmetric harmonic oscillator in cylindrical coordinates. The method also included pairing between nucleons in the BCS approximation with fixed gap parameters for protons and neutrons which were determined phenomenologically from the odd-even mass differences through a symmetric

five-term formula involving the experimental binding energies.

For odd-A nuclei, the fields corresponding to the different interactions were obtained by doing one iteration from the closest even-even nucleus selecting the orbital occupied by the odd nucleon according to the experimental spin and parity. For those cases where this experimental assignment was not well established the orbital closer to the Fermi level was chosen.

In order to describe Gamow-Teller transitions, the spin-isospin residual interaction was added to the mean field. This interaction contained two parts: particle-hole (ph) and particle-particle (pp) interactions. The (ph) part is responsible for the position and structure of the GT resonance. The (pp) part is a neutron-proton pairing force in the $J^\pi = 1^+$ coupling channel.

Theoretical predictions using the methods described above have been shown to reproduce experimental results reasonably well. A comparison between the calculations and experimental results can be found in [Sar01-1]. For example, the calculated Q_{EC} and Gamow-Teller strength agree very well with the measured values in the case of ^{76}Sr as well as in the case of light Kr isotopes [Urk98, Ham99].

3.3 Superallowed $0^+ \rightarrow 0^+$ β decay

According to the conserved vector current (CVC) hypothesis, the matrix elements of the superallowed Fermi β transitions between the (J^π,T) = (0^+,1) states should all be equal, independent of the nuclear structure apart from the small terms for nucleus dependent radiative correction and Coulomb correction. Therefore, the experimental ft values corrected with the above mentioned terms allow an accurate determination of the weak vector coupling constant G_V. The corrected ft value, denoted Ft, and G_V are related as

$$Ft = ft(1+\delta_R)(1-\delta_C) = \frac{K}{2G_V^2(1+\Delta_R^V)}, \tag{8}$$

where $K/(\hbar c)^6 = 2\,\pi^3 ln2\hbar/(m_e c^2)^5 = 8120.270(12)\cdot 10^{-10}$ GeV^{-4} s, f = statistical rate function, t = partial half-life, δ_R = calculated radiative correction, δ_C = total Coulomb correction and Δ_R^V = nucleus independent radiative correction. [Tow02]

The precise determination of Ft, together with the muon decay data, provides a value for the up-down quark mixing matrix element V_{ud} in the Cabibbo-Kobayashi-Maskawa (CKM) matrix.

$$V_{ud}^2 = \frac{K}{2G_F^2(1+\Delta_R^V)\overline{Ft}}, \tag{9}$$

where G_F is a weak coupling constant from muon decay: $G_V = G_F V_{ud}$. The $\overline{Ft}$ is an average Ft value obtained from precisely known superallowed decays. Presently, the largest part of the uncertainty in the value of the V_{ud}^2 is due to the calculated corrections, mainly from δ_R and δ_C.

The value for V_{ud}^2 can be used to test the unitarity of the first row of the CKM matrix:

$$V_{ud}^2 + V_{us}^2 + V_{ub}^2 = 1, \tag{10}$$

where the values V_{us} and V_{ub} are obtained from the K_{e3} decay and B meson decay, respectively. The result, $0.9740(5)^2+0.2196(23)^2+0.0036(10)^2=0.9968(14)$ fails the unitarity test by 2 standard deviations. Recent measurements suggest that the adopted value for V_{us} may be too low [She03]. This new value for $V_{us} = 0.2272(23)$ restores the unitarity, 0.9999(16). Since the failure in the unitarity of the CKM matrix would imply new physics beyond the standard model it is important to eliminate possible trivial explanations for the discrepancy.

The leading term in the sum, V_{ud}^2, includes calculated corrections. In order to restore unitarity, the radiative corrections should either be shifted downwards as much as one quarter of their current value or the Coulomb corrections should shift upwards more than one half of their current value or a combination of these two. However, the leading terms in radiative corrections are very well founded. Therefore, the attention has been focused on the Coulomb corrections. Although smaller than the radiative corrections, the Coulomb corrections are sensitive to nuclear structure because the Coulomb and charge dependent nuclear forces destroy the isospin symmetry between the initial and final analog states in superallowed β decay. [Tow02]

The total Coulomb correction can be separated into two terms:

$$\delta_C = \delta_{IM}^1 + \delta_{RO}, \tag{11}$$

where δ_{IM}^1 = Coulomb mixing component and δ_{RO} = radial non-overlap of the wave functions. The δ_{RO} is due to the fact that the radial wave functions of the converting proton and the corresponding neutron differ because their binding energies are not identical. The δ_{IM}^1 is caused by different degrees of configuration mixing in the wave functions of the members of the isospin multiplet. For a superallowed $0^+ \rightarrow 0^+$ β decay the analog initial and final states are both subject to isospin mixing due to the presence of charge dependent forces. The mixing permits vector β decay to non-analog 0^+ states which are forbidden unless those states contain an admixture of analog configuration. Thus, the magnitude of such non-analog branches reflects the information of the isospin mixing correction δ_{IM}^1. [Hag94]

The value of δ_{IM}^1 can be extracted by measuring the non-analog transition strength and corresponding Q-values for analog and non-analog transitions. In the case of a single non-analog transition, the relation between these quantities is

$$\delta_{IM}^1 = \frac{f_0 b_1}{f_1 + f_0 b_1}, \tag{12}$$

where b_1 is the non-analog branching ratio and f_0 and f_1 are statistical rate functions for analog transition and for non-analog transition, respectively [Hag94].

The required precisions for meaningful tests for the half-life, decay Q-value and branching ratio are $5{\cdot}10^{-4}$, 10^{-4} and 10^{-3}. So far, high enough precisions have been reached in nine decays, ^{10}C, ^{14}O, ^{26m}Al, ^{34}Cl, ^{38m}K, ^{42}Sc, ^{46}V, ^{50}Mn and ^{54}Co. Recently, a decay study reaching such a precision has been published on ^{22}Mg β decay [Har03]. The half-life for ^{74}Rb has been measured with high enough precision but the branching ratios are not yet known accurately. The main source of uncertainty is the expected strong feeding of 1^+ levels in ^{74}Kr, only a part of which has been observed experimentally. For more details, see chapter 5.1 in this work and [Pie03].

3.4 Mirror decays

The mirror β decay between $M_T = 1/2$ and -1/2 states provides an ideal laboratory for studying fine details of nuclear properties. In the mirror decay, initial and final states should have identical wave functions due to the charge symmetry of nuclear forces. These decays are characterised by fast Fermi and Gamow-Teller decays and short half-lives caused by high decay energies determined by Coulomb energy differences. As these transitions are strong, they can be easily identified and, therefore, the comparison of experimental and theoretical Gamow-Teller strengths of individual transitions becomes possible [Mar96]. So far, mirror decays have been studied with high precision only up to ^{59}Zn. (See [Oin97] and the references therein.)

In the A = 70-80 region, the breaking of isospin symmetry starts to play a significant role. It has been suggested that it may even alter the ordering of the low-lying states [Urk98, Oin97]. Furthermore, the deformation effects may drastically affect the Gamow-Teller strength distribution [Fri95, Sar01-1]. The role of deformation on Gamow-Teller strength can be summarised in two types of effects. Firstly, due to deformation, the Gamow-Teller strength distributions corresponding to deformed nuclear shapes are more fragmented than the corresponding spherical ones. Secondly, the levels of deformed orbitals coming from different spherical shells cross each other in a manner depending on the magnitude of the quadrupole deformation and oblate or prolate characteristics of the decaying nucleus. In some cases, this level crossing may lead to sizeable differences between Gamow-Teller distributions corresponding to different shapes of the parent nucleus. The mirror decay of ^{75}Sr measured in this work is the heaviest mirror system in which a detailed decay study has been performed so far. In addition, as the Gamow-Teller decay to the high lying excited states of ^{75}Rb turned out to have an intensity of some percent, this nucleus is a highly promising case for studying deformation effects via GT β decay.

3.5 β delayed proton emission

β decay of proton rich nuclei to the excited states is followed by either a γ emission or a charged particle emission. Far from stability where decay energies are high β

decay can lead to high lying states above the proton separation energy. Also, proton separation energies are not high for nuclei far from stability.

The particle emission is a strong interaction process and, therefore, a faster process than the γ emission. Furthermore, the partial widths for the γ-ray emission are small for the levels above the proton separation energy. This is why the β-delayed particle emission is expected to dominate when approaching the proton dripline. The selection rule for a β-delayed proton decay follows from the conservation of the angular momentum and can be written

$|J_i - J_f| \pm \frac{1}{2} \leq L \leq J_i + J_f \pm \frac{1}{2}$,

where $\frac{1}{2}$ is the proton spin and subscripts i and f denote for initial and final states, respectively. The parity of the final state is given as $\pi_f = \pi_i(-1)^l$.

In heavy nuclei (A >60), the density of final states for β decay is so high that the individual transitions cannot be distinguished. Therefore, the β delayed proton spectrum has a nearly continuous bell-shape. Furthermore, the level structure of the daughter of the proton decay may not be well known. This is why the measured proton intensities can only be used to discuss average features of the decay in question. For example, the Gamow-Teller strength distribution can be extracted as has been done for the ^{75}Sr decay in this work. However, this statement has to be treated with caution due to the limited sensitivity of γ-ray detection.

4 Astrophysical rp-process above Z = 32

In the extreme temperature and density conditions prevailing in X-ray bursts and supernovae, nuclear reaction time scales can be of the order of tens of seconds. The reaction flow in these conditions is called explosive hydrogen burning. In relatively low temperatures and densities the reaction flow can proceed up to the HCNO cycle. When the temperature increases due to energy relese in nuclear reactions, a rapid proton capture process is ignited and can proceed in suitable conditions up to the Sn region [Bro02]. Figure 8 presents a calculated rp-process path.

In addition to nuclear structure studies, the experimental data on the decay properties and masses of proton rich nuclei can be used in astrophysical reaction flow calculations. Recently, Schatz et al. [Sch98] have performed an extensive study of reaction parameters for the rapid proton capture process above Z = 32 up to the A = 100 region. Due to lack of experimental information on proton rich nuclei the calculations have been performed relying mostly on theoretical values of masses and half-lives. However, these calculations clearly indicate the need for complete reaction network calculations for reproducing the observed abundance patterns of elements in astrophysical objects. In particular, Schatz et al. emphasize the role of a two-proton capture in bridging the waiting points of the rp-process towards A = 100 [Sch98].

The 36 <Z <40 region is known to be rich in isomers and deformations. Compared

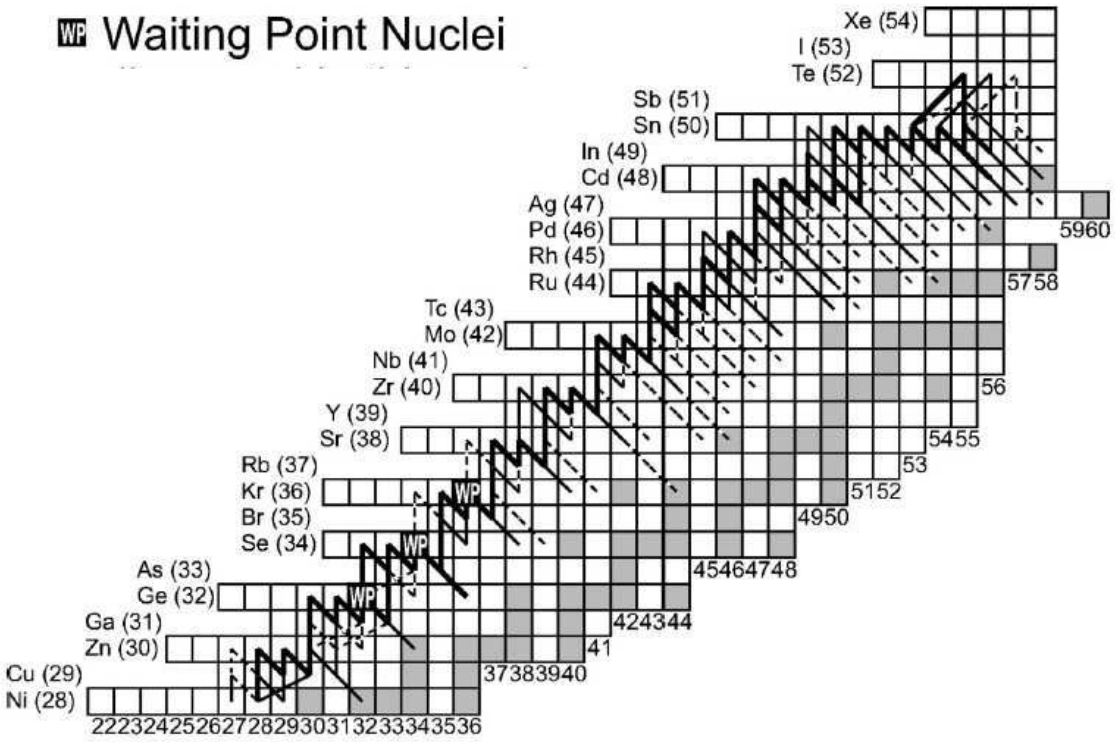

Figure 8: The rp-process path [Bro02]. The thick solid line represents a flow rate higher than 10 %. The thin solid line shows 1-10 % flow rate whereas the dashed line shows a flow rate of 0.1-1 %. The figure also points out the most important waiting point nuclei.

to spherical nuclei deformed nuclei have different single particle levels and additional collective degrees of freedom which increse the level density. The deformation is an important parameter in mass models. As the level density, single particle levels and mass are needed to calculate β-decay half-lives and nuclear reaction rates, the deformation has to be taken into account. In addition, the statistical rate function (eq. 7) depends on the excitation energy as $(Q_\beta - E)^5$. As the different mass models show increasing deviations from each other when moving towards more exotic systems, mass measurements are necessary in this region. Furthermore, β-decay half-lives are crucial as they determine the time structure of the reaction flow as well as the abundance pattern. The large number of isomers in this mass region have a significant role as they affect the half-lives and proton capture rates.

The nuclei studied in this work; ^{74}Rb, ^{75}Sr, and ^{80m}Y are located on the main rp-process path. As ^{74}Rb and ^{75}Sr have short half-lives, β decay dominates their role

in the rp-process. In addition, the intensity of the β-delayed proton decay of ^{75}Sr is relatively small. Therefore, the speed of the reaction flow in this region is mainly determined by ^{76}Sr, a possible waiting point nucleus. Furthermore, as ^{81}Nb is proton unbound [Sch98], the main reaction flow proceeds through ^{80}Zr as well as through ^{80m}Y. The proton capture rate on ^{80m}Y is possibly enhanced compared to that of the ground state of ^{80}Y.

5 Results and discussion

5.1 ^{74}Rb

The level sructure of ^{74}Kr is known well only for the low lying states. Spins and parities for these states have originally been identified in in-beam studies of ^{74}Kr. The first evidence of a 0^+ isomeric state at 508 keV was published by Chandler et al. [Cha97]. Becker et al. measured γ-e$^-$ coincidencies. They detected 495 keV conversion electrons and 694 and 1233 keV γ rays in coincidence, and proposed two 2^+ states above the 0^+ isomer [Bec99]. Bouchez et al. also measured conversion electrons and γ-rays in coincidence with implanted ^{74}Kr ions. This experiment resulted in an improved half-life for the 508 keV isomer and relative intensities for the conversion electrons and a 456 keV γ transition [Bou03].

The attached article [A2] describes the half-life and non-analog branching ratio measurements of ^{74}Rb. In addition, the possible β-delayed proton branch was searched for and as no protons were seen the branching ratio was deduced to be smaller than $5{\cdot}10^{-5}$ per ^{74}Rb decay. No γ transitions were reported. However, a careful re-analysis of the data showed a weak 456 keV transition. No other γ transitions could be found from the data. Therefore, a separate measurement using 2 MINIBALL germanium detectors and a cylindrical scintillator was carried out in 2002. As the γ efficiency was higher and the yield better than in the previous experiment, the E2 branching ratio could be determined. In addition, two other γ transitions were assigned to the ^{74}Rb decay. As there were 6 Ge crystals in use, a search for γ-γ coincidencies was also possible.

Figure 9 shows the γ spectra observed for the ^{74}Rb decay in the 2002 experiment. The gating with the cycle TDC strongly reduced the long living daughter activities as well as the only isobaric contaminant, the ^{74}Ga activity. Due to the lack of veto detectors in this set-up, the background was still fairly high even at the 1.2 MeV region. Therefore, transitions weaker than $4{\cdot}10^{-4}$ per ^{74}Rb decay were not seen. Furthermore, the 52 keV transition de-exciting the 508 keV state to the 456 state was below the threshold of Ge detectors. Recently, the branching ratio for this transition has been measured in a fragmentation experiment in Ganil [Bou03]. The result, $b_{E2}/b_{E0} = 1.2$, differs significantly from the results obtained in a β decay work: $b_{E2}/b_{E0} = 0.7$ [Pie03].

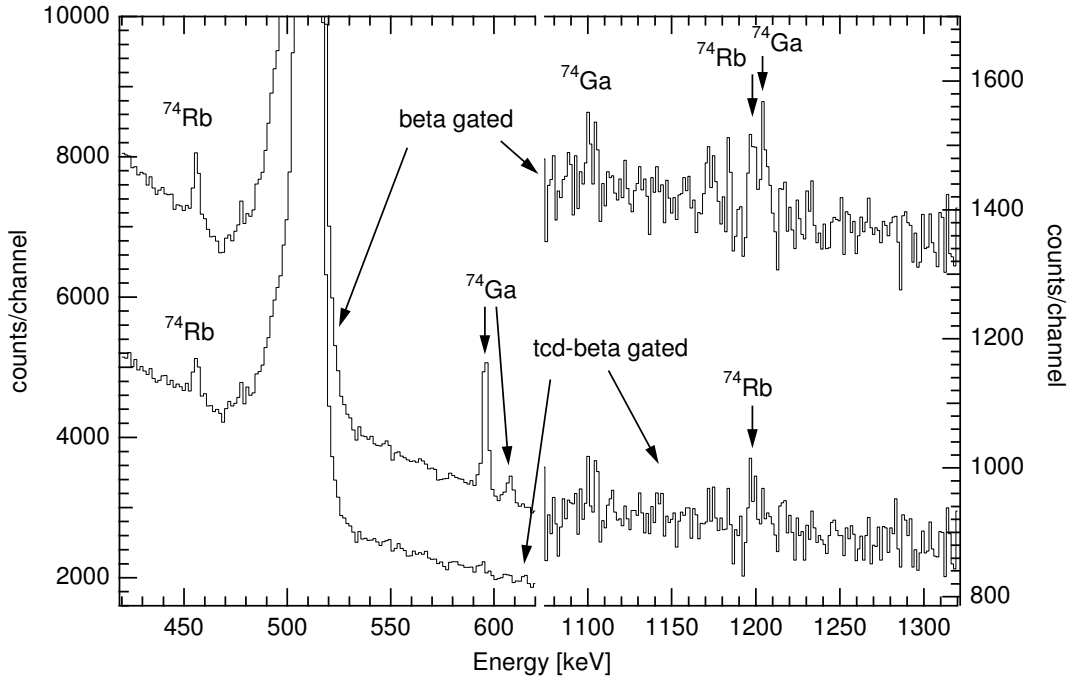

Figure 9: γ spectrum of ^{74}Rb decay. The long living background has been subtracted from the tdc-beta gated spectrum. As can be seen, this reduces the ^{74}Ga activity significantly.

In the present work, the 1198 keV transition was found to be in coincidence with the 456 keV E2 transition. The peak intensities for the 1198 keV line in the β-γ spectrum and in the γ-γ spectrum are similar within errors after efficiency corrections. Thus, the 1198 keV γ transition leads to the ground state via the 2^+ state at 456 keV. However, the initial state cannot be fixed with this data. Figure 10 present a γ spectrum which is a result of gating by the 456 keV transition.

Figure 11 presents the decay scheme of ^{74}Rb based on the experimental information of this work and references [Pie03, Bou03]. A significant fraction of the intensity of the 456 keV E2 transition is due to β feeding to high lying states of ^{74}Kr. The TRIUMF result showed that the 456 keV γ rays are in coincidence with low energy β-particles corresponding to β feeding of levels around 4 MeV [Pie03]. Such a scheme is supported by the shell model calculation which predicts more than 400 1^+ states at high energies [Har02]. These states are favourably fed in allowed GT transitions. Furthermore, γ ray intensities are not in balance in the decay scheme shown in Figure 11, showing that the 456 keV 2^+ state has to be fed by presently unobserved transitions from the higher lying levels.

The existence of another excited 0^+ state at 1654 keV shown in Figure 11 is not

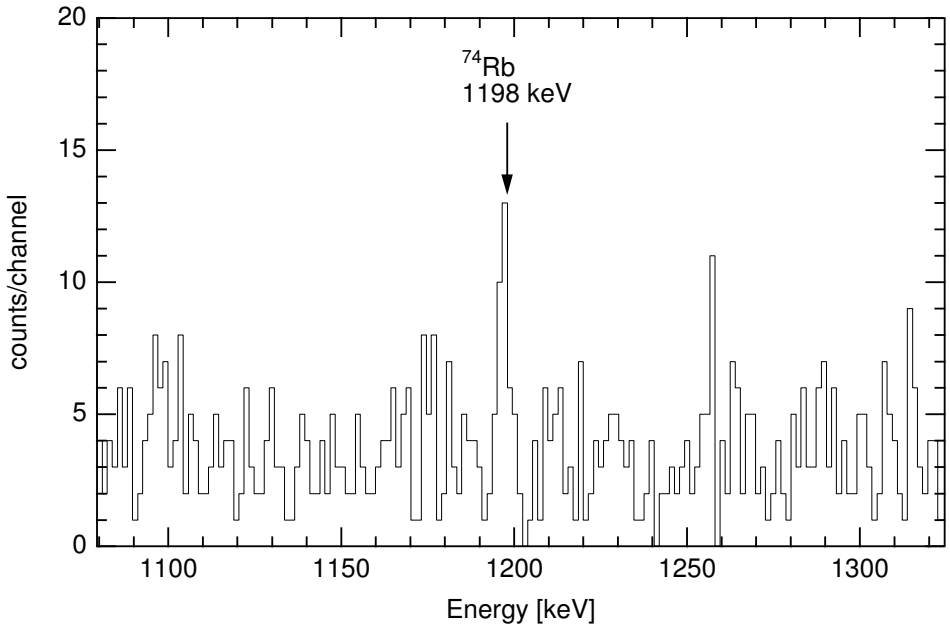

Figure 10: A γ-ray spectrum peak in coincidence with the 456 keV transition. It shows a clear 1198 keV transition in the ^{74}Rb decay.

confirmed. It is even possible that the 1198 keV transition results from a higher lying state and the de-exitation proceeds to the first 2^+ state via several intermediate states. Thus, there would be several γ transitions on the way and as they are weak, they are lost in the background. However, there is evidence that most of the 1198 keV γ rays are due to β feeding to levels at about 2 MeV [Pie03]. Additional support for this assignment is provided by the shell model calculations which predict a 0^+ level at 1918 keV [Pie03]. No other clear γ-γ coincidences were detected. The β-γ and γ-γ spectra showed several weak "peaks" which, however, could not be assigned to any transition in the known level scheme. Table 2 presents transition intensities as measured in this work and in [Pie03].

The measurement of the non-analog branching ratio allowed the determination of the magnitude of the Coulomb mixing component δ^1_{IM}. The upper limit obtained in this work using the branching ratios presented in Figure 11,δ^1_{IM} <0.08 %, is only slightly larger than what has been measured for lower mass nuclei. The calculated values 1.4 - 3.1 % [Orm95] seem to be unrealistically large when compared to the present experimental upper limit.

As pointed out in chapter 3.3 the largest individual uncertainty of the average $\overline{Ft}$ value is due to the total Coulomb correction δ_C. In the absence of the required precision to test the CKM matrix, the present results can be used to extract information on δ_C. Assuming the validity of the CVC hypothesis and using the adopted $\overline{Ft}$ value

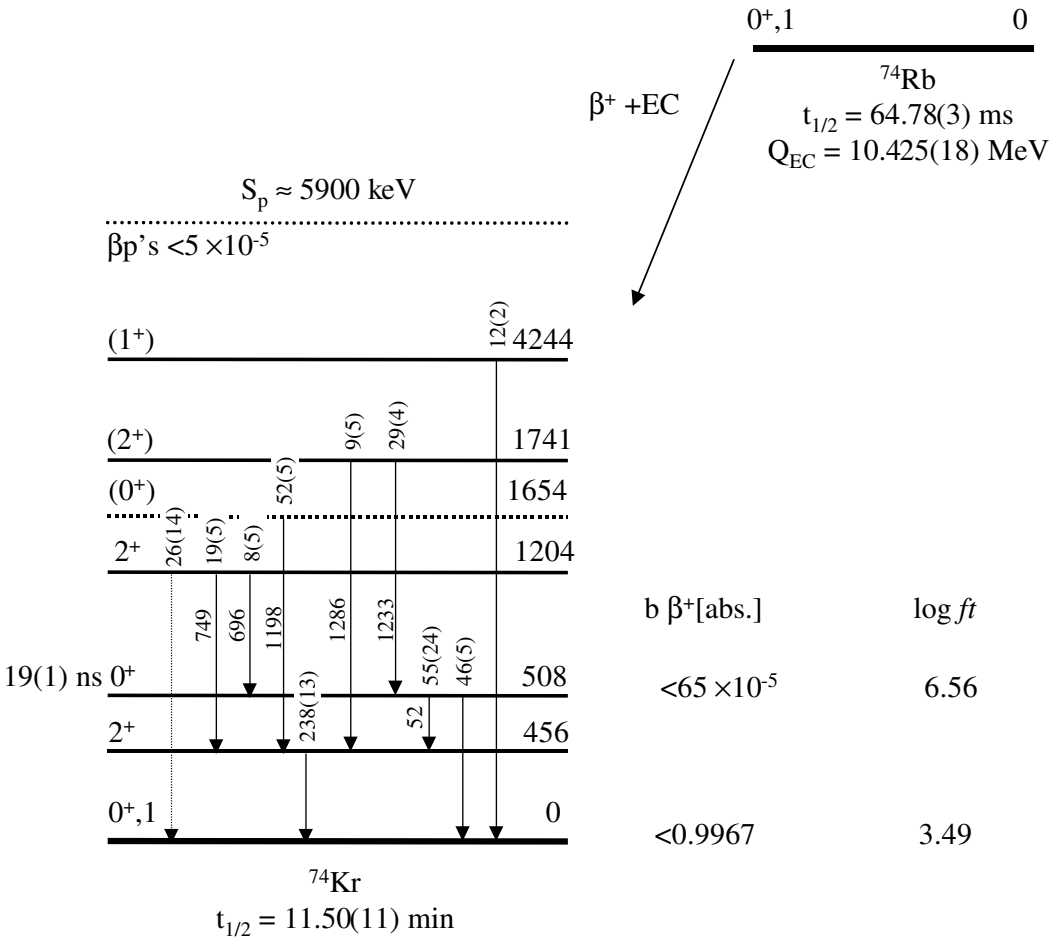

Figure 11: ^{74}Rb decay scheme. The transition intensities shown in units of 10^{-5} per ^{74}Rb decay and the half-life are the weighted averages from this work and [Pie03]. The existence of a 0^+ level at 1654 keV is not confirmed. The Q_{EC} value was measured in a separate experiment using the ISOLTRAP [Her02]. The half-life and the E2/E0 ratio for the 508 keV 0^+ isomer were recently measured in a fragmentation experiment [Bou03].

of 3072.2(8) and the experimental results presented in this thesis, the value for δ_C can be calculated using equation 8. The result, 2.4(3) %, is in agreement with the value presented in [Kel02] but as the information on branching ratios has improved since the uncertainty is smaller by a factor of 3. In addition, this value is in agreement with the theoretical prediction which suggests that the total Coulomb correction should increase to about 2 % for A >60 nuclei [Har98].

Table 2: The β-decay of ^{74}Rb.

Energy [keV]	Assignment	Intensity per 10^5 ^{74}Rb decay	
		this work	TRIUMF [Pie03]
52	$0^+ \rightarrow 2^+$	$<16^n$	32(7)
456	$2^+ \rightarrow 0^+$	180(30)	250(14)
508	$0^+ \rightarrow 0^+$	37(11)	48(5)
696	$2^+ \rightarrow 0^+$	$<10^n$	8(5)
748	$2^+ \rightarrow 2^+$	$<10^n$	19(5)
1198	$(0^+ \rightarrow 2^+)$	50(20)	52(5)
1204	$2^+ \rightarrow 0^+$	$<10^n$	26(14)
1233	$(2^+) \rightarrow 0^+$	40(20)	29(4)
1286	$2^+ \rightarrow 2^+$	$<10^n$	9(5)
4244	$(1^+ \rightarrow 0^+)$	$<20^n$	12(2)

n = no visible peak, upper limit

5.2 ^{75}Sr

The β-decay half-life of ^{75}Sr measured in this work, 88(3) ms, is in agreement with the previously published results, 71^{+71}_{-24} ms [Bla95] and 80^{+400}_{-40} ms [Kie01]. Its uncertainty, however, is smaller by an order of magnitude.

The present experiment measured the β-delayed γ ray de-exciting the ^{75}Rb level for the first time. The transition intensity for a 144 keV γ ray was measured to be $4.5^{+1.9}_{-0.7}$%. The asymmetric errors are due to possible internal conversion. This transition was assigned to be a $(5/2^-)$ level of ^{75}Rb de-exciting to the ground state. The log *ft* values deduced for the 144 keV level and the ground state are 5.0 and 3.7, respectively. The stronger transition to the ground state suggests a superallowed character. Therefore, J^π of the ground-state of ^{75}Sr has to be the same as that of the ^{75}Rb ground state. If we adopt spins and parities from [Gro97], the ^{75}Sr ground state must have $J^\pi = (3/2^-)$. The theoretical work by Hamamoto [Ham99] supports this assignment. The β + EC delayed proton decay branching ratio was measured to be 5.2(9)%.

The measured Q_{EC}-value, 10.60(22) MeV, supports the value obtained from the FRDM calculation, 10.7 MeV [Sch98], and from the mass systematics from [Aud95], 10.6$\pm$0.3 MeV.

Among the isospin multiplets Q_{EC} can be estimated using the relation

$$\Delta E_C = M(T, M_T) - M(T, M_T + 1) + \Delta_{NH} = Q_{EC} + \Delta_{NH}, \qquad (13)$$

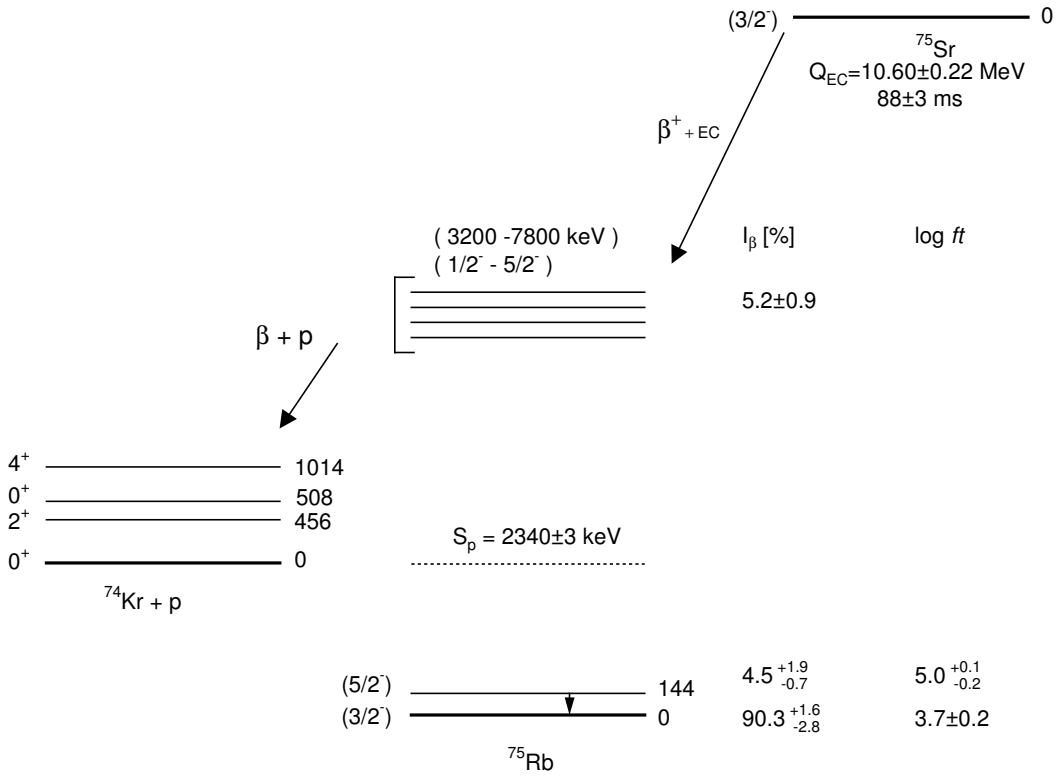

Figure 12: ^{75}Sr decay scheme.

where ΔE_C is the Coulomb displacement energy, Ms are the masses of the neighbouring isobaric analog states and Δ_{NH} is the mass difference between neutron and hydrogen. Figure 13 presents the Coulomb displacement energies for T = 1/2 ground states. The value for ^{75}Sr is from the measurements of the present work. The rest are from [Ant97] except ^{57}Cu, ^{59}Zn and ^{65}As which are taken from [Aud95], ^{61}Ga from [Wei02] and ^{71}Kr from [Oin97]. The solid line is a fit with the following function

$$\Delta E_C = 1348.5(1)\frac{\overline{Z}}{A^{\frac{1}{3}}} - 644.9(2), \tag{14}$$

where A is the mass number and $\overline{Z}$ is the average charge of the elemental pair [Ant97]. The agreement between the measured values and values obtained from the systematics is excellent. Table 3 presents the ΔE_C-values calculated using equation 14.

According to the theoretical calculations which assume prolate deformation for ^{75}Sr, the $|\langle\sigma\tau\rangle|$ is expected to be larger than that for ^{71}Kr. For ^{75}Sr β decay, the calculated

Table 3: Coulomb displacement energies.

Isotope	ΔE_C [keV] Calculated	Measured	Reference
^{61}Ga	9804	10037(50)	[Wei02]
^{71}Kr	10917	10920(320)	[Oin97]
^{75}Sr	11348	11380(220)	this work

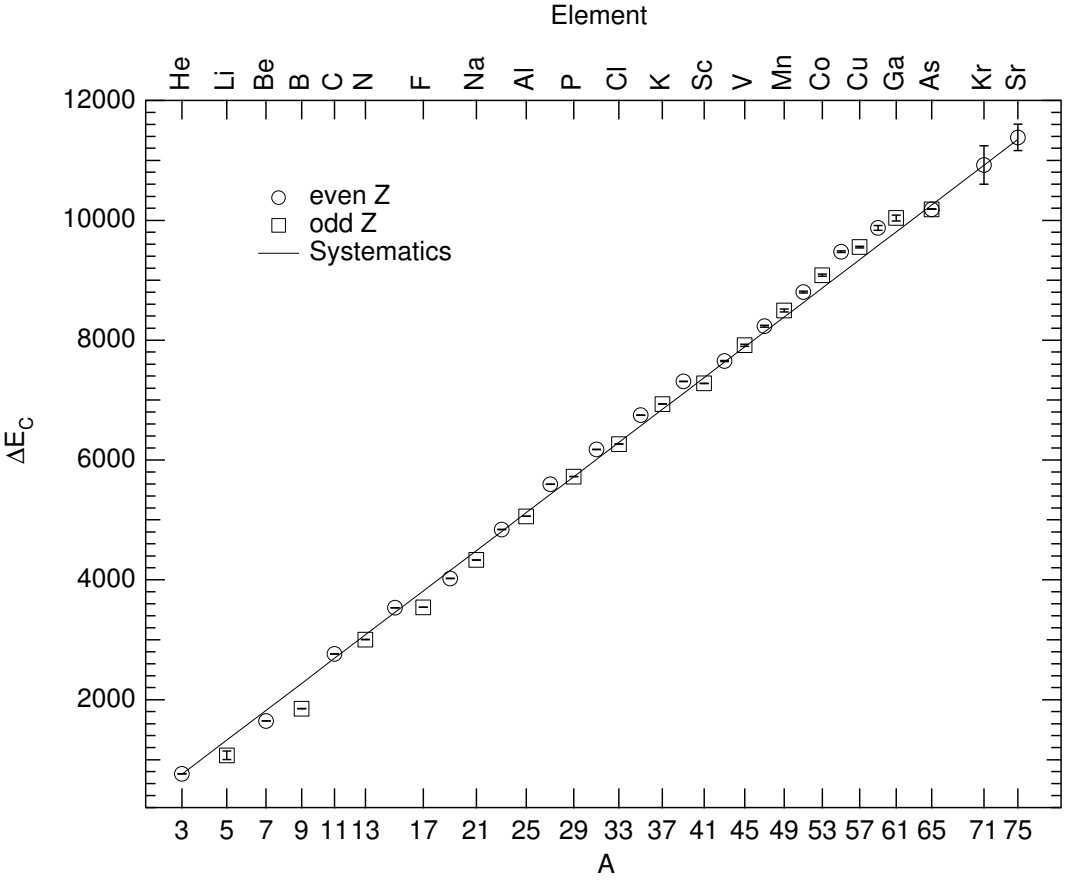

Figure 13: Coulomb displacement energies for T = 1/2 ground states. The literature cut-off date for [Ant97] data is Oct. 1. 1996. Therefore, ^{61}Ga, ^{71}Kr and ^{75}Sr were not included in the fit of equation 14 in [Ant97].

$|\langle\sigma\tau\rangle|$ values are ≤ 0.54 and ≤ 0.44 for the mirror transition and for the transition to the first excited state, respectively [Ham99]. The $|\langle\sigma\tau\rangle|$ values measured in this work are 0.35(5) and $0.20^{+0.04}_{-0.02}$ for the ground state and the first excited state (eq. 7). The

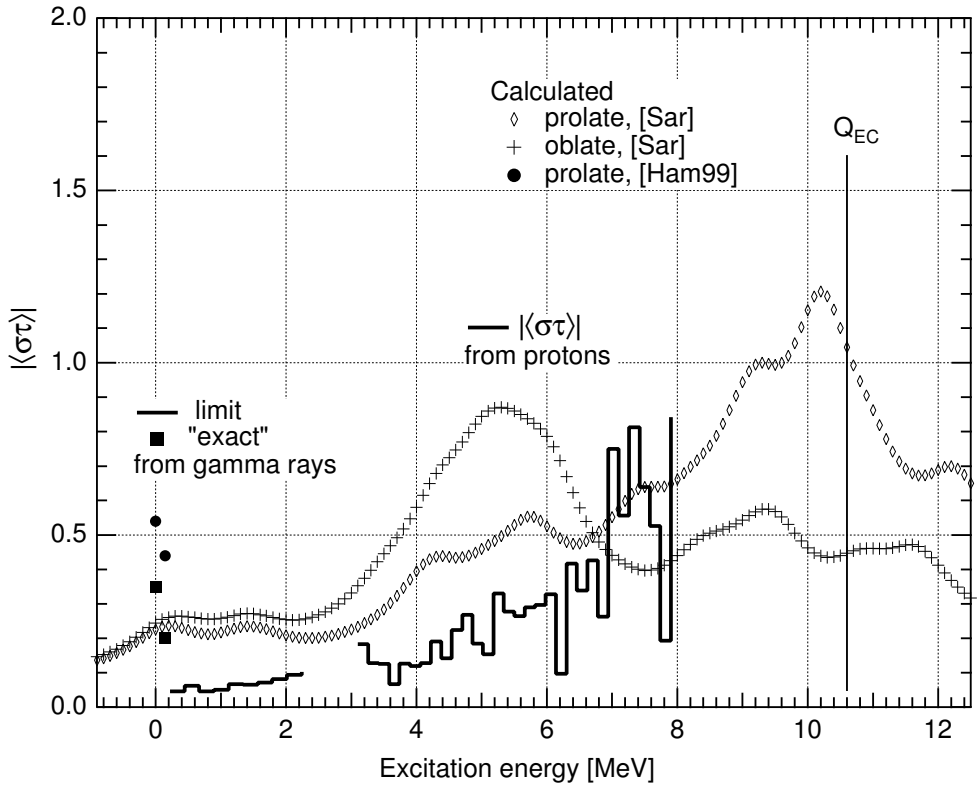

Figure 14: Gamow-Teller strength. Due to low statistics, the uncertainties on the values extracted from the proton spectrum are as high as 30-50 %. The $|\langle\sigma\tau\rangle|$ extracted from the γ-ray spectrum represents a sensitivity limit as no transitions were observed.

$|\langle\sigma\tau\rangle|$-value for the ground state transition follows the systematic trend measured for the lower mass nuclei [Oin97]. This can be expected as the $|\langle\sigma\tau\rangle|$-value is expected to reach its minimum in the middle of the closed shells due to the collective effects.

Figure 14 presents the Gamow-Teller strength distribution obtained in the ^{75}Sr experiment. The values deduced from the γ-ray spectrum have to be taken as the upper limits as no other transitions except 144 keV were seen in the experiment. The calculation of the theoretical curves [Sar] and points [Ham99] follow the procedure described in chapter 3.2.

The low-energy part of the GT strength distribution in odd-A N$\sim$Z nuclei is due to 1-quasiparticle excitations involving the single odd neutron [Sar01-2]. The higher-energy part is mainly due to more collective excitations and can possibly be used to distinguish between oblate and prolate deformations of a nucleus [Sar01-1]. The experimentally observed β-delayed proton spectrum seems to probe the high-energy part of the GT-strength distribution which directly populates 3-quasiparticle induced states

in ^{75}Rb. The trend of the measured GT-strength seems to favour prolate deformation. However, the interpretation of these results is limited by low statistics in the proton spectrum.

The gap seen in the experimental curve is caused by the β background in the FUTIS array which prevented the identification of protons below 0.7 MeV and which corresponds to the excitation energy of 3.1 MeV. However, the gain of the Ge detector used for γ rays was set to cover the region only up to 2.2 MeV. Furthermore, the Coulomb barrier reduces the emission of low energy protons.

5.3 ^{80}Y

The rp-process nucleosynthesis is generally delayed by the β decay of even-even N = Z nuclei. In particular, the β decay of ^{80}Zr controls the reaction flow towards the A $\sim$ 100 region as the proton capture is hindered due to the negative binding energy of proton unbound ^{81}Nb [Res00]. This is why the half-life of the β decay daughter of ^{80}Zr, ^{80}Y has a significant role.

The lifetime of ^{80}Y is small during most of the rp-process due to fast proton capture reactions. When the temperature starts to decrease it becomes a critical parameter as proton capture rates are lower. During freezeout, the ^{80}Y β decay and proton capture are competing, thus, determining the amount of A = 80 nuclei in the rp-process reaction flow and also the number of stable ^{80}Kr produced in the rp-process.

The discoveries of the isomers in ^{80}Y, a 4 μs 2^+ state at 312 keV [Reg97] and a 4.7(3) s 1^- state at 228 keV [Dör98] have increased the interest on this nucleus as the isomers play an important role in the rp-process. The proton capture rates and the β decay life-times can significantly differ for the isomers and for the ground states.

^{80}Y studied in the present work was produced using the HIGISOL-SPIG system. The reaction used was ^{54}Fe(^{32}S,3p3n)^{80}Y. The beam energy was 150 MeV and the thickness of the enriched ^{54}Fe target was 2.7 mg/cm^2. In order to obtain a clean sample of ^{80}Y, the SPIG was used with a low dissociation voltage, e.g. voltage between the SPIG and the stoppping volume. Therefore, ^{80}Y was accelerated and mass separated as YO$^+$ ions, appearing at mass 96. This provided a factor of 24 suppression on the isobaric background. The production rate of ^{80m}YO was 3.6 atoms/second.

In the present experiment, a confirmation was obtained that the 84 keV isomeric transition is located above the 228 keV state. In addition, the 228 keV transition was confirmed to be an isomeric transition in ^{80}Y using β-γ and e$^-$ $-$ γ coincidencies. The internal conversion coefficient was determined from the e$^-$/γ ratio and from the KX/γ ratio measured using ELLI and a Ge detector. The weighted average of these two measurements gave a value of α_K = 0.50(7) for the K-conversion. This is consistent with the M3(+E4) multipolarity for the 228 keV isomeric transition and results in I^π = 1^- for this state. The half-life for the isomer was determined as a weighted average of the 228 keV γ ray, yttrium X-rays and conversion electron measurement. The result,

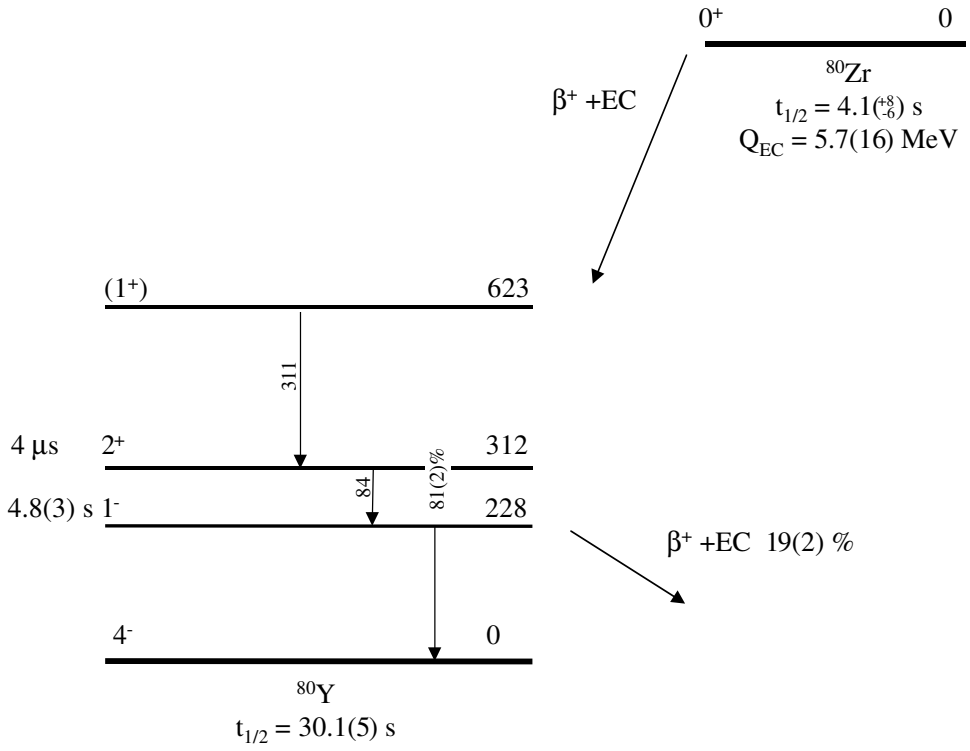

Figure 15: ^{80m}Y decay scheme. EC + β^+ decay branching ratio for the isomer decay is from [Dör98].

5.0(5) s, is also in agreement with the earlier result 4.7(3) [Dör98]. The weighted average of these two values for the half-life is 4.8(3) s.

The ground state of ^{80}Y has been assigned to have $I^\pi = 4^-$ and the ^{80}Zr ground state has been assigned as $I^\pi = 0^+$ state. Therefore, the β decay of ^{80}Zr will lead exclusively to ^{80m}Y. Thus, the proton capture will occur in the isomeric state and not in the ground state as previously assumed. The partial β decay half-life for the isomer is 25(4) seconds. Therefore, the effective ^{80}Y β decay lifetime is reduced by <17 %. The effect of the isomeric state and β decay half-life reduction on the rp-process reaction flow depends on how different the proton capture rate of the isomeric state is compared to that of the ground state.

6 Summary

The present thesis studied the β decay of ^{74}Rb, ^{75}Sr and ^{80m}Y by means of β-delayed γ-ray and proton spectroscopy. The experiments were performed using the mass separator facilities at ISOLDE at CERN in Geneva and at IGISOL in Jyväskylä. In addition, test experiments both on-line and off-line were performed using the IGISOL facility. The purpose for these tests was to improve the understanding of the processes involved in the ion guide efficiency.

In order to overcome the problem with the large energy spread of the mass separated beam from the ion guide, the use of a sextupole ion guide, SPIG, was studied with the fission and heavy-ion ion guides. The measured results show that the mass resolving power can be improved significantly when replacing the traditional skimmer with the SPIG. The production rates of the radioactive nuclei of the heavy-ion ion guide were slightly increased and the yields of the fission ion guide showed significant improvement.

The effect of a ring electrode between the skimmer and the ion guide exit hole was studied using the light-ion ion guide. The conclusion from these tests was that with the ring electrode the transmission efficiency between the skimmer and the exit hole can be maintained despite the large current flowing out from the ion guide. As a result, production rates were improved as the efficiency did not drop when increasing the primary beam intensity.

The global properties of the ion guide system were studied using a ^{223}Ra α-recoil source. These studies consisted of delay time and efficiency mesurements as a function of ion guide pressure, source-to-exit-hole distance as well as buffer gas purity. The result obtained was that the buffer gas purity should be matched to properties of the ion-of-interest. The proof of this is the measured charge state distribution of evacuated ions which can be influenced by the amount of impurities in the buffer gas.

The ^{223}Ra α-recoil source was used to test the idea of injecting electrons inside the stopping volume and, thus, improving the evacuation efficiency. An off-line test carried out showed that a significant increase of the efficiency can be achieved. However, on-line tests are required to measure whether this positive effect is present also with the presence of the plasma created by the ionising radiation.

The superallowed β decay of ^{74}Rb was studied in order to measure the intensity of the allowed Gamow-Teller decay to the high lying excited states of ^{74}Kr as well as the non-analog branching ratio to the first excited 0^+ state. Furthermore, the γ-γ coincidence measurement was conducted for the first time. As a result, a 1198 keV transition was confirmed to belong to this decay and de-exciting to the ground state of ^{74}Kr via the first excited 2^+ state at 456 keV. The measured non-analog branching ratio allowed the estimate of the magnitude of the Coulomb mixing component. The result was significantly smaller than theoretical predictions. The total Coulomb correction $\delta_C = 2.4(3)$ % deduced using the experimental results presented in this thesis agrees with the theoretical predictions, suggesting that the radial overlap part of the Coulomb

correction is larger than expected.

The heaviest mirror system studied so far, the β decay of ^{75}Sr, extends the systematics of mirror decays to a region of large deformations. The β-delayed γ transition belonging to the β decay of ^{75}Sr was detected for the first time. The half-life of ^{75}Sr was measured with improved accuracy and the β-delayed proton intensity was confirmed. The measurement of the proton spectrum allowed the estimate of the Gamow-Teller distribution of this decay. In addition, this result supports the prediction of prolate deformation for ^{75}Sr ground state.

The conversion electrons de-exciting the ^{80m}Y were measured and allowed the determination of the spin and parity of the isomeric state. In addition, it was confirmed that the 84 keV isomeric transition is located above the 228 keV isomeric transition in the decay scheme. These results show that the β decay of ^{80}Zr leads to the population of the isomeric state of ^{80}Y. Consequently, the proton capture during the rp-process takes place in the isomer, not in the ground state as assumed earlier in the reaction flow calculations.

References

[Ant97] M. S. Antony et al., Atomic data and nuclear data tables 66 (1997) 1.

[Aud95] G. Audi and A. Wapstra, Nucl. Phys. A 595 (1995) 409.

[Bec99] F. Becker et al., EPJ A 4 (1999) 103.

[Bla95] B. Blank et al. Phys. Lett. B 365 (1995) 8.

[Bou03] E. Bouchez et al., Phys. Rev. Lett. 90 (2003) 082502.

[Bri99] P. Bricault et al., Proceedings of 15th International Conference on Cyclotrons and their Applications (Cyclotrons '98) Caen, France, Institute of Physics Publishing (1999) 347.

[Bro02] B. A. Brown et al., Phys. Rev. C 65 (2002) 045802.

[Bru77] B. J. Brussaard and P. W. M. Glaudemans, Shell-Model Applications in Nuclear spectroscopy, North-Holland, Amsterdam (1977).

[Cha97] C. Chandler et al., Phys. Rev. C 56 (1997) R2924.

[Did94] F. Didierjean and G. Walter, CRN report no. CRN PN 94-01 (1994).

[Den00] P. Dendooven et al., Czec. J. of Phys. Vol 50/S1 (2000) 235.

[Dör98] J. Döring et al., Phys. Rev. C 57 (1998) 1159.

[Ebe96] J. Eberth et al., Nucl. Instr. Meth. A369 (1996) 135.
http://www.ha.physik.uni-muenchen.de/okester/rex/

[Ewa81] G. T. Ewan et al., Nucl. Phys. A 352 (1981) 13.

[ISO00] D. Forkel-Wirth and G. Bollen (eds.), Hyperfine Interactions 129 (2000).

[Fri95] F. Frisk et al., Phys. Rev. C 52 (1995) 2468.

[Gro97] C. J. Gross et al. Phys. Rev. C 56 (1997) R591.

[Hag94] E. Hagberg et al., Phys. Rev. Lett. 73 (1994) 396.

[Ham99] I. Hamamoto, Phys. Rev. C 60 (1999) 011305.

[Har98] J. C. Hardy and I. S. Towner, in: C. Baktash (Ed.), Proceedings of Conference Nuclear Structure, Gatlinburg, AIP Conference Proceedings, Vol. 481, Amer. Inst. Phys., New York, 1998.

[Har02] J. C. Hardy, I. S. Towner, Phys. Rev. Lett. 88 (2002) 252501.

[Har03] J. C. Hardy et al., Phys. Rev. Lett. 91 (2003) 082501.

[Her02] F. Herfurth et al., Eur. Phys. J. A 15 (2002) 17.

[Hon97] A. Honkanen et al., Nucl. Instr. and Meth. Phys. Res. A 395 (1997) 217.

[Hua03] W. X. Huang et al., Europhys. Lett., 63 (2003) 678.

[ISOLDE] http://isolde.web.cern.ch/ISOLDE/

[Kan95] J. Kantele, Handbook of Nuclear Spectrometry, Academic Press, London (1995).

[Kel02] A. Kellerbauer, PhD thesis, A Study of the Accuracy of the Penning Trap Mass Spectrometer ISOLTRAP and Standard-Model Tests With Superallowed Beta Decay, University of Heidelberg, (2002).

[Kie01] P. Kienle et al. Prog. Part. Nucl. Phys. 46, (2001) 73.

[Lil01] J. Lilley, Nuclear Physics: Principles and Applications, John Wiley & sons (2001).

[Mar96] G. Martinez-Pinedo et al. Phys. Rev. C 53 (1996) R2602.

[Oin96] M. Oinonen et al. JYFL Annual report (1996) 16 and H. Fynbo et al. Nucl. Phys. A 677 (2000) 38.

[Oin97] M. Oinonen et al., Phys. Rev. C 56 (1997) 745.

[Orm95] W. E. Ormand and B. A. Brown, Phys. Rev. C 52 (1995) 2455.

[Par91] J.-M. Parmonen, et al. Nucl. Instr. and Meth. Phys. Res. A 306 (1991) 504.

[Pie03] A. Piechaczek et al., Phys. Rev. C 67 (2003) 051305(R).

[Reg97] P. H. Regan et al., Acta Phys. Polonica B 28 (1997) 431.

[Res00] J. J. Ressler et al., Phys. Rev. Lett. 84 (2000) 2104.

[Roe03] E. Roeckl et al., Nucl. Instr. and Meth. Phys. Res. B 204 (2003) 53.

[Sar01-1] P. Sarriguren, Nucl. Phys. A 691 (2001) 631.

[Sar01-2] P. Sarriguren et al., Phys. Rev. C 64 (2001) 064306.

[Sar] P. Sarriguren, to be published.

[Sch98] H. Schatz et al., Phys. Rep. 294 no. 4 (1998).

[Sch95] K. Schreckenbach et al., Phys. Lett. B 349 (1995) 427.

[She03] A. Sher et al., arXiv:hep-ex/0305042 (2003).

[Tas89] P. Taskinen et al., Nucl. Instr. and Meth. A 281 (1989) 539.

[Tow95] I. S. Towner et al., ENAM 95 proceedings, (1995) 711.

[Tow02] I. S. Towner, J. C. Hardy, Phys. Rev C 66 (2002) 035501.

[Urk98] P. Urkedal and I. Hamamoto, Phys. Rev. C 58 (1998) R1889.

[Wei02] L. Weissman et al., Phys. Rev. C 65 (2002) 44321.

[Wil78] D. H. Wilkinson et al., Phys. Rev. C 18 (1978) 401.

[Ärj81-1] J. Ärje and K. Valli, Nucl. Instr. and Meth. 179 (1981) 533.

[Ärj81-2] J. Ärje et al., Nucl. Instr. and Meth. 186 (1981) 149.

[Ärj83-1] J. Ärje et al., Proc. Int. Ion Eng. congress ISIAT'83, Kyoto (1983) 583.

[Ärj83-2] J. Ärje, Physica Scripta, T3 (1983) 37.

[Äys84] J. Äystö et al., Phys. Lett. B 138 (1984) 369.

[Äys01] J. Äystö, Nucl. Phys. A 693 (2001) 477.